Rotor Blade-Vortex Interaction Impulsive Noise Source Localization

W. R. Splettstoesser* and K. J. Schultz*
DFVLR Braunschweig Research Center, Braunschweig, Federal Republic of Germany
and
Ruth M. Martin†
NASA Langley Research Center, Hampton, Virginia

An acoustic source localization scheme applicable to noncompact moving sources is developed and applied to the blade-vortex interaction (BVI) noise data of a 40% scale BO-105 model rotor. A generalized rotor wake code is employed to predict possible BVI locations on the rotor disk and is found useful in interpreting the acoustic localization results. The highly varying directivity patterns of different BVI impulses generated at the same test condition is explained by both the localization results and predicted tip vortex trajectories. The effects of rotor tip-path-plane angle and advance ratio (at otherwise constant parameters, respectively) on the BVI source positions is studied. Decreasing tip-path-plane angle moves the general interaction region upwind on the rotor disk, significantly changing the interaction geometry. Increasing advance ratio shifts the general source region downwind on the rotor disk with the increased convection of the vortices until about 60-deg azimuth, where the BVI sources appear to become acoustically less effective. The region of strongest BVI sources lies beween 60- and 70-deg azimuth and 80 and 90% radius for the moderate range of advance ratios studied.

Nomenclature

C_T = rotor thrust coefficient
c = speed of sound, m/s
D = distance source—observer, m
M_H = hover tip Mach number
R = rotor radius, m (=2 m)
r = radial distance from rotor hub, m
T_M = observer time, s
T_S = source time (time when noise is emitted), s
T_T = time when blade trigger signal is released, s
t = time, s
V = freestream velocity, m/s
X = streamwise coordinate of tunnel fixed system, with origin at rotor hub, positive upstream, m
Y = cross-stream coordinate, positive toward advancing side, m
Z = vertical coordinate, positive above hub
x,y,z = rotor fixed coordinate system, (x,y parallel to tunnel fixed system X,Y,Z), m
α_{TPP} = rotor tip-path-plane angle, positive nose up, deg
γ = blade-vortex intersection angle, deg
ψ = azimuth angle in the tip-path plane, deg (zero over tail, 90 deg over rotor advancing side)
μ = advance ratio, $= V\cos\alpha_{TPP}/\Omega R$
τ = retarded time, s
Ω = angular speed of rotor, rad/s

Subscripts

M,mic = microphone, observer
S = noise source
W = traversing wing microphone position

Presented as Paper 87-2744 at the AIAA 11th Aeroacoustics Conference, Sunnyvale, CA, October 19–21, 1987; received May 9, 1988; revision received Nov. 1, 1988.

*Research Scientist, Technical Acoustics Division, Institute for Design Aerodynamics.
†Research Engineer, Aeroacoustics Branch. Associate Member AIAA.

Introduction

HELICOPTER blade-vortex interaction (BVI) impulsive noise has in recent years become a topic of great importance in helicopter acoustics research. When it occurs, BVI noise dominates the acoustic signal and is in the frequency range considered the most important to human subjective response. The impulsive noise is the result of the aerodynamic interaction of a rotor blade with the trailing vortex system generated by preceding blades. The phenomenon is predominantly generated during low-speed descent, when the separation distance between the rolled-up blade tip vortices and the rotor plane is extremely small. Since the interactions are highly dependent on the wake characteristics, the occurrence of this phenomenon is very sensitive to rotor design and helicopter operating conditions.

Previous research into rotor BVI noise has been aimed at defining the rotor operating regimes when BVI noise is important, the most important parameters for BVI noise generation, the scalability of BVI signals from model to full scale, the directivity of BVI noise sources, and the locations of the BVI noise sources.[1–8] Results from a recent BVI acoustics test program[9–10] have shown that the BVI acoustics directivity patterns are strongly dependent on operating conditions. Both the character of the directionality and the primary directions of strongest radiation were found to vary greatly in the low-speed range of rotor advance ratio $\mu = 0.075–0.170$. The lowest μ cases ($\mu = 0.075–0.09$) exhibited multiple, equal, but low-amplitude acoustic interactions per blade and weakly directional acoustic radiation patterns. The higher μ cases ($\mu = 0.116–0.146$) exhibited sharper, fewer, and higher amplitude interactions per blade and a sharply focused directivity lobe. The results suggested that the changing directivity characteristics are due to changes in the interaction geometry, which in turn are due to changes in the rotor- wake geometry and the locations where BVI occurs. To pursue these ideas, the present investigation into the BVI source locations was undertaken.

The present paper will concentrate on the identification of the BVI source locations on the rotor disk for a large range of moderate-speed test conditions. An investigation is made into the changes in the interaction geometry with the rotor tip-path-plane angle (at constant advance ratio) and with the rotor advance ratio (at constant tip-path-plane angle). The

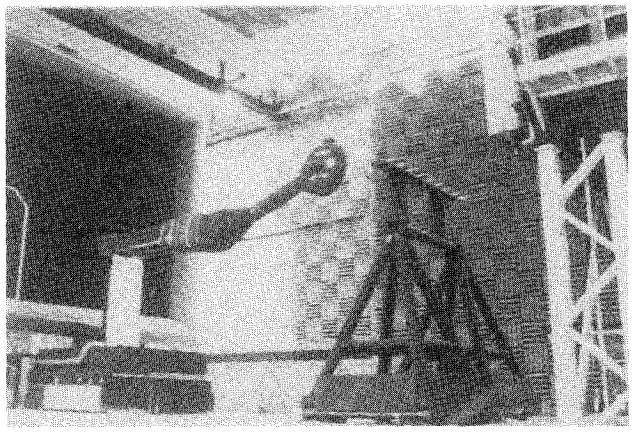

Fig. 1 Sting-mounted model rotor test rig and traversing microphone array installed in the DNW open test section.

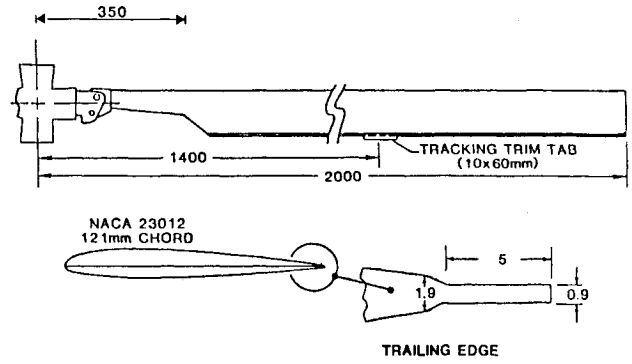

Fig. 2 Geometry of BO-105 model rotor blades.

empirically found BVI source locations are also compared with the results of the United Technologies Research Center (UTRC) generalized wake program.[11-12] The predicted wake geometry is found to be a useful tool in interpreting the results of the acoustic source identification.

Experimental Apparatus and Procedures

The acoustic data employed for this work were acquired during a joint NASA/DFVLR experiment performed in the open-jet test section of a large German-Dutch aero-acoustic test facility, the Duits-Nederlandse Wind Tunnel (DNW), using a 40% dynamically scaled model of the MBB BO-105 helicopter main rotor.

The DFVLR rotor test stand is shown sting mounted in the 6×8 m DNW open-jet test section in Fig. 1. The test stand is fully described in Ref. 13, and the details of data acquisition and reduction of the rotor performance data are given in Refs. 14 and 15. During this test, the rotor test stand was housed within an acoustically insulated fiberglass shell. The sting was covered with a streamlined sound absorptive lining to minimize reflections.

Model Rotor

The rotor is a 40%, dynamically scaled model of the four-bladed, hingeless BO-105 main rotor (Fig. 2). The rotor blade is constructed of a NACA 23012 airfoil, with the trailing edge modified to form a 5-mm-long tab to match the geometry of the full-scale rotor. Further details are given in Table 1 and Ref. 13.

The nominal rotor operating speed was 1040 rpm, giving an acoustic blade passage frequency of about 70 Hz and a nominal hover tip Mach number of 0.64.

Acoustic Instrumentation

The acoustic instrumentation consisted of a nine-microphone inflow array mounted on a traversing system and two inflow microphones attached to the rotor fuselage as shown in Fig. 3. The microphones were 0.5-in. "pressure"-type condenser microphones equipped with standard nose cones. The array vertical position was 2.1 m below the hub, thus allowing noise measurements upstream and below the rotor plane over a total range of 8.2 m (see Figs. 1 and 3). The microphone "wing" and the supporting structure were covered with open-cell foam material to minimize sound reflections.

Table 1 Details of the DFVLR BO-105 model main rotor

Rotor diameter	4 m
Blade chord	0.121 m
Blade airfoil section	NACA 23012
Number of blades	4
Blade tip speed	218 m/s
Lock number	4.47
Rotor thrust coefficient	0.0044
Blade solidity	0.077
Blade twist	−8 deg

Acoustic Data Acquisition and Reduction

Before recording on analog tape, the microphone signals were high-pass filtered at 4 Hz to remove very low frequency content. Two blade position reference signals (1/revolution and 512/revolution) were also recorded with the acoustic signals. All microphone channels and blade reference signals were then conditionally digitized using a sample rate keyed to the 512/revolution signal, which yielded 1024 data points/revolution or a sample rate of about 18,000 samples per second. An antialiasing filter was employed at 9 kHz. Forty revolutions of the time histories were digitized in this manner and then averaged to obtain an average acoustic waveform and standard deviation.

Testing Procedures

Corrections to the freestream flow angle and speed due to the presence of the lifting rotor in the test section were calculated according to the method of Heyson[16] and applied to the measured data off-line to obtain the corrected tip-path-plane angles presented here.

The rotor parameters tip-path-plane angle, hover tip Mach number, and thrust were set using the digital displays at the rotor controls. The rotor operator "flew" the rotor to zero the first harmonics of the shaft bending moments, so that the first harmonics of lateral and longitudinal flapping were close to zero. Neglecting blade bending, the measured rotor shaft angle is thus equivalent to the tip-path-plane angle.

A full documentation of the test program, model test rig, instrumentation, data acquisition and reduction, in addition to a large representative set of the averaged acoustic signals are given in Ref. 10.

Tip Vortex Trajectory Predictions

Patterns of possible blade-vortex interaction regions were obtained from the stand-alone version of the UTRC generalized wake module.[11-12] This wake geometry generalization includes only the effect of axial wake distortion and uses a classical helical wake description for the in-plane coordinates. Reference 11 notes that compared to the axial distortions, the in-plane distortions are not large near the rotor plane, so that this simplification is reasonable.

It should be noted that there are several differences between the generalized rotor geometry and the BO-105 rotor, namely the BO-105 twist (−8 deg), Lock number (4.47), aspect ratio (18), and airfoil section (NACA 23012). The most important of these is probably the difference in twist. Fairly large differences in the axial tip vortex coordinate are predicted for

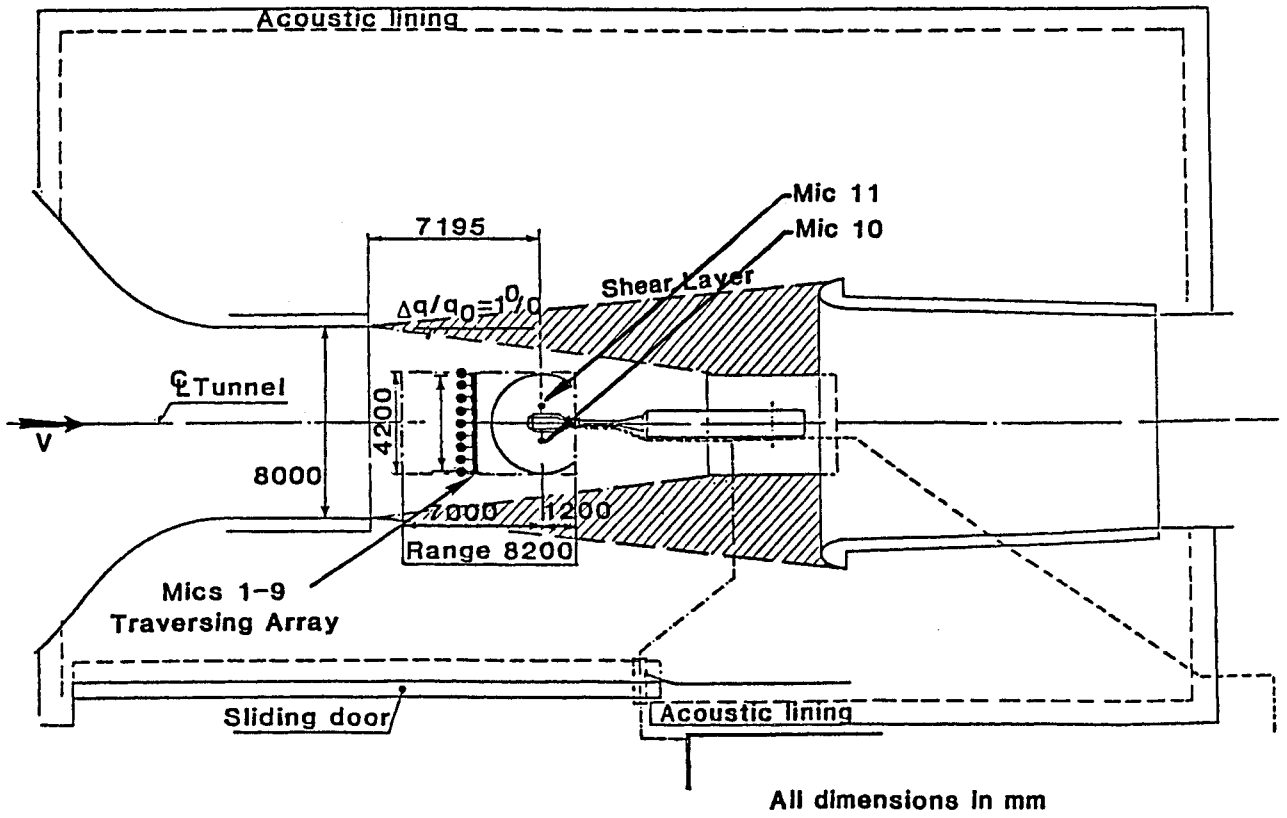

Fig. 3 Diagram of experimental apparatus in the DNW open test section (top view).

blades with −10- and −14-deg twist, as illustrated in Ref. 11. The influence of Lock number was found to be not important for performance prediction, and aspect ratio was not found to be a secondary wake geometry parameter.

For each C_T, μ, α_{TPP}, and coning angle, the tip-vortex coordinates for specific azimuthal locations ψ (every 5 deg) and rotor revolutions (4) are calculated. The rotor is divided into a grid according to specified radial and azimuthal steps (0.05 R and 5 deg), and the tip-vortex coordinates are searched to locate close proximity to the blade. The proximity criterion requires that, at a particular point on the blade, the vortex must be within a specified x, y (0.05 R) and z distance (0.10 R or 1.7 chord), accounting for the vertical displacement of the blade due to coning. When a BVI is identified, the intersection angle with respect to the blade leading edge is calculated using the two closest tip-vortex coordinates. The radius, azimuth, vertical distance, intersection angle, vortex number, and vortex age are then calculated. Vortex age is expressed in degrees of azimuth since the vortex was created. Intersection angles are defined as 0 and 180 deg for a parallel interaction, and 90 and 270 deg for a normal interaction.

BVI Source Localization Technique

Since it is known that BVI sources are noncompact extended sources, the conventional triangulation technique (which is a mathematically exact method for compact point sources) was not applied. The source localization approach employed here does not require the assumption of a point source or that of a stationary source emitting the total noise radiation. It is postulated that the BVI noise originates from the rotor plane close to the rotor blade leading edge. Making use of the measured total time between the 1/revolution trigger signal and the arrival times of a characteristic BVI pressure pulse denoted A in Fig. 4 at the individual micro-

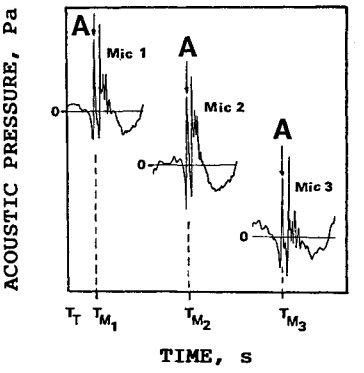

Fig. 4 Example of a typical BVI acoustic signal (impulse A, measured at three microphones).

phones, the geometric locations of possible noise sources along the blade's leading edge—as it rotates—are calculated for each microphone. More specifically, the technique consists of balancing the total measured time delay ($T_M - T_T$), with the time ($T_S - T_T$) required for the blade to rotate from the trigger azimuth position (blade pointing downstream as in Fig. 5) to the source position S and the time τ required for the sound to propagate from the source to the observer (microphone) position M, yielding

$$T_M = T_S + \tau \tag{1}$$

This simple expression combines the known geometric and temporal quantities with the unknown radial and azimuthal source coordinates r_S and ψ_S in the rotor fixed coordinate system. With $T_S - T_T = \psi_S/\Omega$, where $\tau = D/c$, and D is the noise propagation path $\overline{SM}$ (also accounting for the convec-

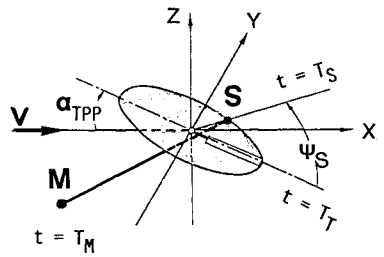

Fig. 5 Diagram of acoustic source localization technique geometry.

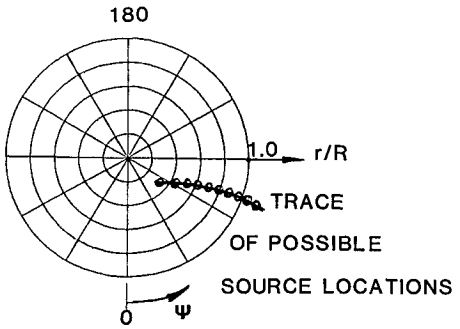

Fig. 6 Trace of possible source locations.

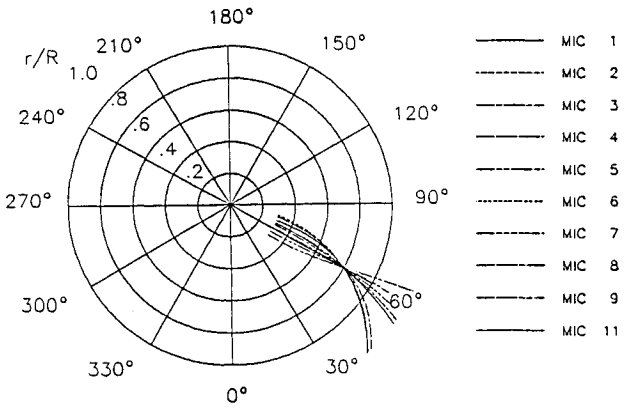

Fig. 7 Test case for source localization technique ($\mu = 0.138$, $\alpha_{TPP} = 5$-deg, 2-deg coning angle) using 10 microphones and known source position ($r_S/R = 0.80$, $\psi_S = 60$ deg).

tive tunnel flow), Eq. (1) can be written to solve for the source azimuth coordinate

$$\psi_S = (T_M - T_T - D/c)\Omega \qquad (2)$$

Since the sound propagation path D is a function of both ψ_S and r_S, Eq. (2) is implicit in ψ_S and has to be solved iteratively for specified values of r_S. This was performed for a number of arbitrarily assumed radial source coordinates along the blade span. The resulting pairs of source coordinates are plotted in the polar diagram of Fig. 6 and form a trace of possible source locations in the rotor plane. Each point of this trace may contribute acoustic energy to the peak amplitude (noted A in Fig. 4) of the microphone under consideration.

Repeated application of this procedure for different microphones (see Fig. 4) yields different traces of possible source locations, one for each microphone as illustrated in Fig. 7. The intersection or close approximation of these lines represents the center of the BVI source area.

Checkout of the Source Localization Code

The new source localization technique was first checked

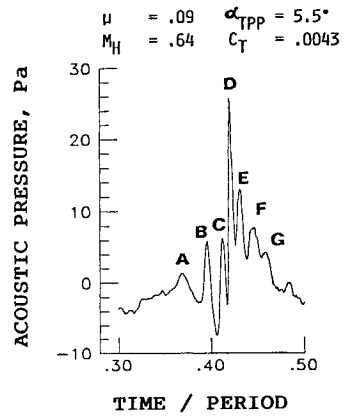

a) Acoustic time history of microphone 6 showing seven BVI impulses, A—G

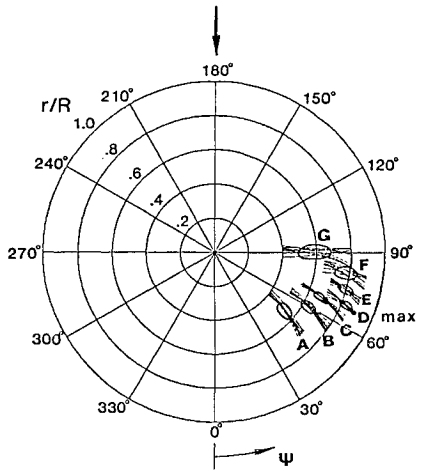

b) Localization results for impulses A—G.

Fig. 8 Localization of multiple BVI sources at $\mu = 0.09$, $\alpha_{TPP} = 3.3$ deg, $C_T = 0.0044$, $M_H = 0.64$, $X_W/R = 0.75$.

using a prescribed compact source at 80% radius and 60-deg azimuth. The result for 30-m/s flow velocity, 5-deg tip-path-plane angle, and 2-deg coning angle is shown in Fig. 7, where the traces for nine wing microphones (1–9) and the starboard body microphone (11) precisely intersect in the expected source position. The source traces have been extended spanwise past the blade tip for better identification of the intersection point.

In additon, a comparison of the results of the new method with some of the results of an instrumented AH-1 model rotor,[17] where the exact noncompact BVI source locations can be determined from the measured absolute blade pressure time histories, gave confidence in the reliability of this source localization technique.

Repeatability and Estimate of Accuracy

Data points with identical operating conditions that were repeated at different times during testing and measured at identical or different observer locations indicated excellent repeatability of the noise source identification results. The accuracy of localizing the radial source position is estimated to be in the range of 3% radius. Based on the resolution of the angle encoder used for the blade position measurement, the accuracy of the BVI source azimuth localization is estimated to be less than 1 deg.

Multiple BVI Source Identification

The localization was first applied to a low advance ratio case ($\mu = 0.09$) with multiple blade-vortex interactions as

shown in the time history plot of Fig. 8a measured at microphone position 6. When the reference blade (1) passes through the first quadrant, a total of seven BVI impulses is generated, one of which is very sharp and of high amplitude (D) with three preceding ones (A,B,C) and three following ones (E,F,G). The localization results are presented in Fig. 8b, demonstrating the high resolution of this technique. Even the lower-amplitude impulses (A,E,F,G) are located, although the microphone traces do not converge as closely as the more pronounced peak locations. The maximum BVI peak is generated at about 70-deg azimuth and 85% span, which corresponds to the highest local Mach number of the seven source locations.

BVI Source Localization Results

The source localization code was subsequently applied to a large number of BVI test conditions to study the directivity of individual sources, to investigate the degree of correlation with predictions of a generalized wake code, and to explore changes of the BVI source locations with parametric variations of tip-path-plane angle and advance ratio.

Directivity of Individual BVI Sources

The source localization results confirmed the strong directionality of BVI noise radiation reported earlier in Ref. 9. An example of the dramatic change in BVI waveforms and amplitudes is presented in Fig. 9 of Ref. 18, which also demonstrates the existence of retreating side BVI.

Correlation of Predicted and Measured BVI Source Locations

To allow a direct comparison of the acoustic localization results with the UTRC generalized wake code, the triangulation results are traced on the wake prediction plots as shown in Fig. 9. The wake prediction plots represent the projection of the tip vortices in the tip-path-plane. A symbol represents a possible BVI when a blade is located at that azimuth: thus, the plot represents all possible interactions as a blade moves through one revolution. The four tip vortices are represented by the four different symbols. The symbol size indicates proximity to a blade, taking into account blade coning as was done in the acoustic source localization. The larger the symbol, the closer the vortex is to the blade. The shaded symbols indicate that the vortex is above the rotor, the open symbols indicate the vortex is below the rotor. Thus, the possible interaction locations with a vortex passing through the disk can be observed on the plot. A dot in the center of the open symbols indicates that the vortex was within $\pm 0.005\,R$ of the blade ($\triangleq$ 10 mm).

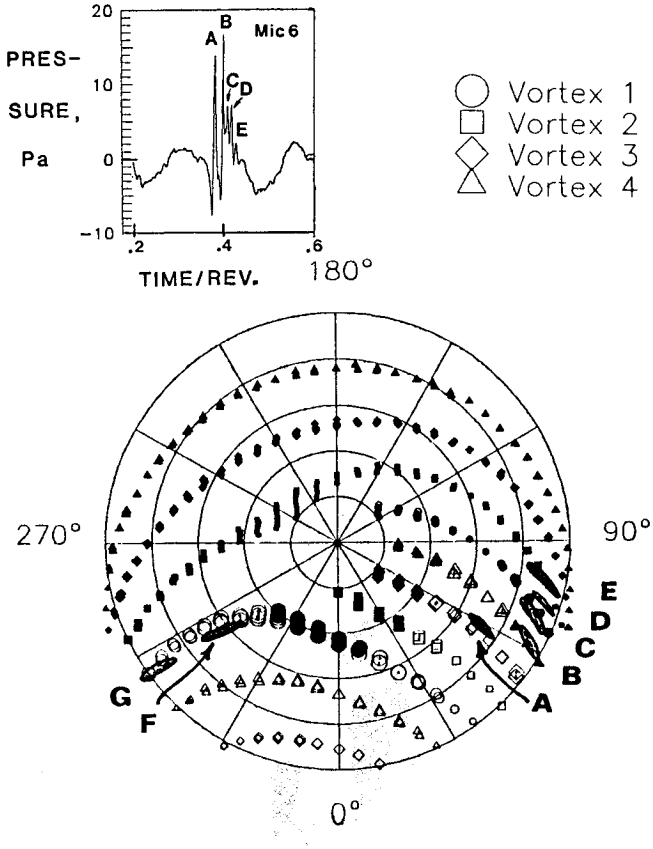

Fig. 9 Comparison of acoustic source locations and tip vortex trajectory predictions at $\mu = 0.15$, $\alpha_{TPP} = -1.4$ deg, $C_T = 0.0044$, $M_H = 0.64$ (Top: related BVI signature at microphone 6).

The triangulation results are superimposed on the wake prediction plots. Advancing (A–E) and retreating side (F,G) BVI noise sources are identified, demonstrating very good agreement with the wake predictions for this test condition simulating 60 knot level flight. However, close proximity of the vortices is predicted at many additional locations on the disk other than the acoustic source locations. It is found that the blade-vortex intersection angles for those locations are close to 90 degrees. Therefore, the aerodynamic interaction region on the blade is small and appears acoustically less effective.

In Table 2, the vertical distance z/R, blade-vortex intersection angle γ, and vortex age (degrees aximuth since the vortex was created) are noted for the vortex filaments nearest to the source locations. The maximum amplitude BVI is generated at location B (about 62-deg azimuth and 90% span) close to the location where the one-revolution-old vortex of blade 4 is predicted to pass through the rotor disk. The intersection angle is predicted to be 150 deg, which is 30 deg from a parallel interaction. Source locations C and D appear to be correlated with the identical vortex created by the same blade (blade 1) one revolution earlier. Such double (twin) sources were observed quite frequently and also can be seen in some of the following figures. One explanation would be the occurrence of two close vortices from one blade. That possibility was recently attributed to a negative tip loading on the advancing side at high-speed flight conditions.[19] Figure 9, however, represents a low-speed (60 knots) level flight condition. An alternate possibility (contributed during the review process) is that the in-plane wake distortions, although generally small compared with the axial distortions, may be significant in these regions of the rotor disk for the purpose of identifying very closely spaced BVI phenomena.

Parametric Effects on Source Locations

Variation of Tip-Path-Plane Angle

The effect of changing the rotor tip-path-plane angle on the individual source locations at $C_T = 0.0044$ is shown in Fig. 10 for a low μ case (= 0.09). The acoustic data were measured at constant observer positions $X_W/R = 1.25$ upstream of the rotor hub and $Z_W/R = 1.05$ below the rotor plane.

In Fig. 10, α_{TPP} was changed from 6 to 2 deg, thus decreasing the descent rate from 2.2 to 1 m/s at a low-speed condition. Excellent comparison of the localization results and in-plane wake predictions is obtained, as shown in Fig. 10a.

Table 2 Interaction geometry for $\mu = 0.15$, $\alpha_{TPP} = -1.4$ deg

BVI	z/R	γ, deg	Vortex age, deg
A	0.02	170	450
B	0.02	150	385
C/D	0.03	135	310
E	0.04	120	235
F	−0.01	350	450
G	−0.02	10	430

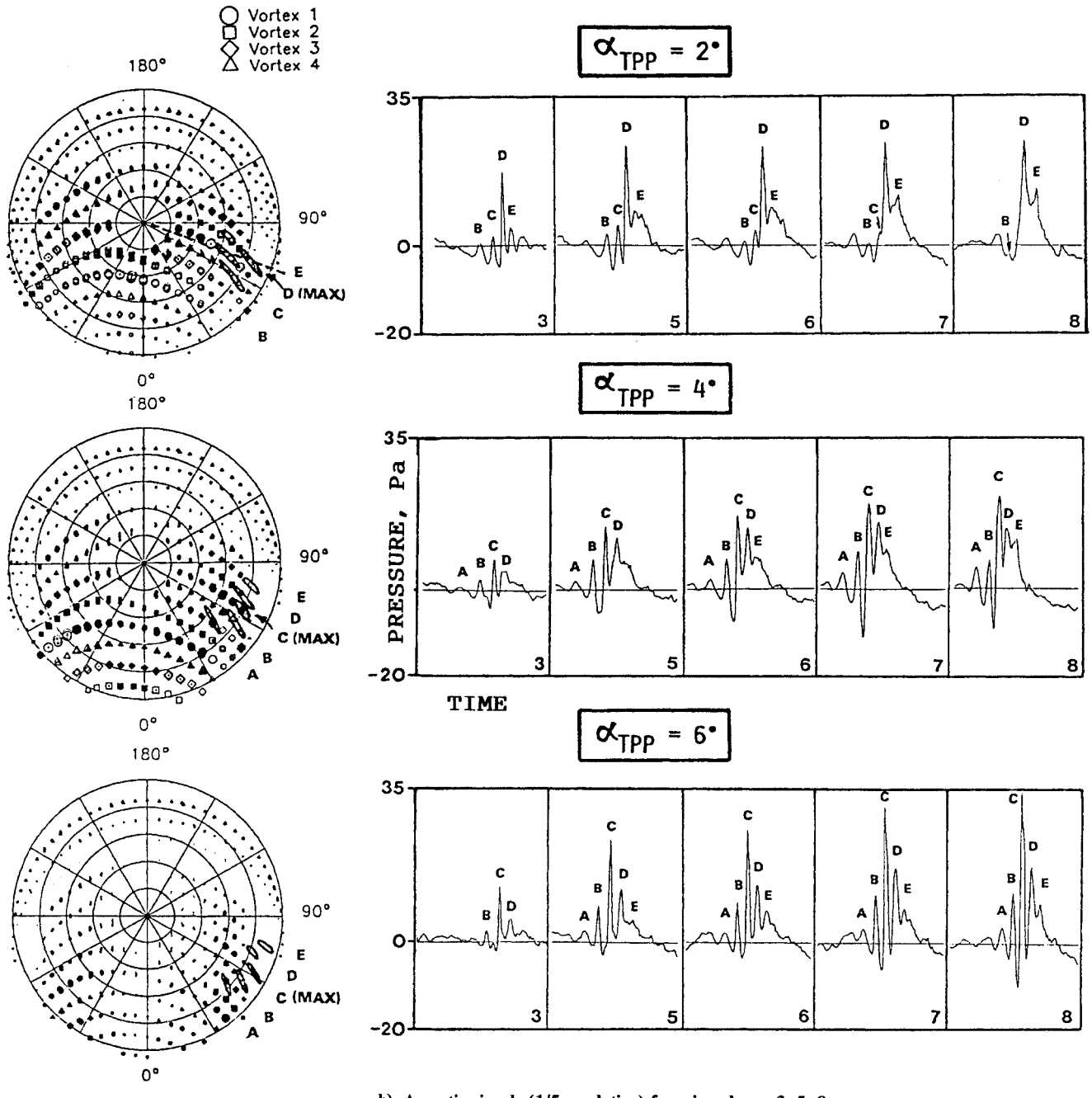

a) Source locations and tip vortex trajectory predictions

b) Acoustic signals (1/5 revolution) for microphones 3, 5–8 measured at $X_W/R = 1.25$

Fig. 10 Effect of tip-path plane angle on BVI locations at $\mu = 0.09$, $C_T = 0.0044$, $M_H = 0.64$.

The different source locations seen in Fig. 10a contribute to the total BVI waveforms shown in Fig. 10b at the different microphones; however, the signals represent the same BVI event. Each BVI source in the rotor plane produces its individual impulse (correspondingly denoted) in the acoustic time history, altogether forming the total BVI signature radiated when a blade passes through the first quadrant. The vertical distance of the vortex to the rotor plane z/R, the blade-vortex intersection angle and vortex age for the individual source locations are given in Table 3. It should be noted that in some cases at high α_{TPP} the vortex z coordinate is predicted far from the rotor disk (> 10% radius): however, the noise measurements still show considerable BVI radiation from the localized sources. This indicates that the wake prediction capability deteriorates at higher positive tip-path-plane angles (increasing descent rates), and in fact the generalization was concentrated on the α_{TPP} range of -6 to 0 deg.

As the rotor is being tilted forward—decreasing the positive tip-path-plane angle and thus decreasing rate of descent—it appears that the general source location region of the maximum BVI impulse and the associated smaller BVI impulses is moving slightly forward in the rotor disk. One possible explanation for the upstream shift of the source locations is that the vortex pattern predicted to be above the rotor plane (shaded symbols) for the high angle of attack starts to pass through the rotor plane when α_{TPP} is decreased (note increasing number of open symbols).

It is very interesting to note in Fig. 10a (upper diagram for $\alpha_{TPP} = 2$ deg) that BVI peaks C and D are being produced by one blade interacting with two vortices (originating from blades 1 and 2, respectively) at nearly the same time but at different locations in the rotor disk, approximately 0.15 R

Table 3 Interaction geometry for $\mu = 0.09$, $\alpha_{TPP} = 2,4,6$ deg

α_{TPP}, deg	BVI	z/R	γ, deg	Vortex age, deg
2	B	−0.03	170	720
	C	−0.02	160	640
	D	0.05	150	570
	E	0.02	150	570
4	A	0.0[a]	180	800
	B	0.0[a]	170	730
	C	0.01	160	640
	D	0.02	150	560
6	A	0.02	180	800
	B	0.03	170	700

[a]Vortex passing through rotor disk.

apart (see dashed line at about 70-deg azimuth). The geometry is such that there is a small noise path difference to the port side microphones, while the noise path is close to identical to the starboard microphones. The related time history plots clearly show the two distinct and separate pulses for C and D at the port side microphone 3, and also at microphones 5 and 6. They are separated by time delays due to the propagation path differences. For microphone 3, a time delay of about 0.58 ms was calculated, which agrees well with the measured time delay of 0.52 ms in the acoustic time history of microphone 3. On the starboard side at microphone 8, the propagation time delay resulting from the noise path difference is only 0.1 ms, so that the small-amplitude BVI peak of source C had merged into the large-amplitude peak D and is no longer visible. The development of this merging process can be traced in the series of time history plots of Fig. 10b. It very nicely explains some of the directivity effects of BVI noise radiation.

Similar observations were made for the moderate advance ratio case of $\mu = 0.17$, as presented in Ref. 18.

Variation of Advance Ratio

The correlation of possible changes in BVI source locations with variation of advance ratio was examined with all other parameters held constant ($\alpha_{TPP} = -1$ deg, $M_H = 0.64$, $C_T = 0.0044$, $X_W/R = 1.25$). The advance ratio was varied over a range of 0.16–0.27, simulating descending flight conditions with increasing speed (66–116 knots) and increasing descent rates (200–1400 ft/min). The results are shown in Fig. 11.

It appears that sometimes one blade interacts with two different vortices at the same time (see B and C at $\mu = 0.19$) or with one vortex at different locations (see C and D at $\mu = 0.18$ and 0.23). Due to noise path differences to the port and starboard side microphones, the earlier mentioned impulse merging process occurs at the starboard measurement locations, contributing to the changing directivity pattern for the total BVI signature.

The in-plane vortex trajectory predictions and source localization results for the maximum impulse BVI sources are in excellent agreement over the advance ratio range measured. It appears that all the higher μ cases (starting at $\mu = 0.18$) at least two impulsive sources are associated with one vortex. One of these interactions occurs a little earlier and more inboard than the other. Again, it appears as if there are two tip vortices originating from the same blade. An alternate argument related to small in-plane wake distortions was discussed earlier.

On close inspection of the individual test cases of Fig. 11, the following interesting trends with increasing advance ratio are observed:

1) At $\mu = 0.16$ (mild descent of 200 ft/min, 66 knots), the maximum amplitude source **B** is located at about 63-deg azimuth and 90% radius and is due to an interaction with the vortex of blade 4, which is approximately one revolution old and is predicted to pass through the rotor plane.

2) At advance ratios of 0.17 and 0.18, source B has moved downstream with vortex 4 past 60 deg and then at higher μ loses stength. At $\mu = 0.18$, the formation of a twin-source appears (C and D correlated with vortex 1).

3) At the next higher μ of 0.19, source C (the first of the twin sources) located at approximately 65-deg azimuth is now the maximum amplitude source location.

4) At $\mu = 0.23$, source D of vortex 1 is the most important contributor and has moved further downstream to about 60-deg aximuth, 80% radius position. Source C has moved more inboard and radiates at lower acoustic intensity. A new source E is now detected, which is correlated with vortex 2.

5) Finally, at the highest-speed, high-descent flight condi-

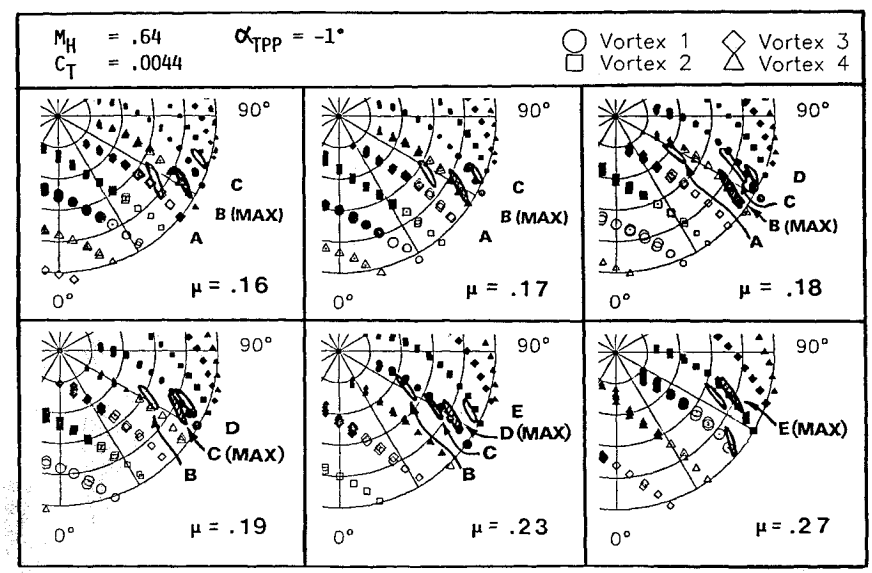

Fig. 11 Effect of advance ratio on BVI locations at $\alpha_{TPP} = -1$ deg, $C_T = 0.0044$, $M_H = 0.64$.

tion $\mu = 0.27$, source E from vortex 2 now has become the dominant source. Compared to the $\mu = 0.23$ case, the maximum amplitude source has "jumped" forward again to about 70-deg azimuth and 80% radius.

Summarizing the above observations, it appears that at increasing advance ratio, the most intense BVI source tends to move between 60- and 70-deg azimuth and 80 and 90% radius, precisely following the convection of the predicted vortex path.

Conclusions

An acoustic source localization scheme applicable to noncompact moving sources was developed. The technique was applied to nearly half-scale rotor BVI data to localize the individual BVI sources and has shown excellent resolution and repeatability.

A generalized wake code was employed to predict possible BVI locations on the rotor disk. The results were correlated with the acoustically determined BVI source locations. The predicted in-plane vortex locations were in excellent agreement with the acoustic source positions. In many cases, the close vertical proximity of the vortices to the rotor disk (a necessary presumption for BVI) also was well predicted, but a generally sufficient correlation was not found. However, the wake code is considered to be an extremely useful tool to interpret the source localizaton results.

Effects of strong directional radiation of different BVI impulses are explained. The interaction of one blade with two (or more) vortices was observed quite frequently and could be used to interpret the merging of individual BVI impulses into one impulse at particular measurement locations. Retreating side BVI source locations were identified close to 300-deg azimuth angle.

The effect of rotor tip-path-plane angle on BVI source location changes was studied. A decrease in tip-path-plane angle with otherwise fixed parameters has shown that the sources move slightly forward in the rotor disk. This movement also leads to interactions with younger vortices and considerable changes in the interaction geometry, implying changes in the acoustic amplitudes and directivity.

Increasing advance ratio with all other parameters held constant was shown to move the most intense BVI source downstream following the vortex trajectory that produces the interaction. When the vortex trajectory is convected downwind past 60-deg azimuth, the most intense source location "jumps" forward in the rotor disk to the predicted vortex trajectory of the preceding blade and the downstream travel with that vortex starts again with further increase in the advance ratio. The maximum amplitude BVI source maintains its position between 60- and 70-deg azimuth and 80 and 90% radius. This location appears to be typical for descending flight since it also was found during the tip-path-plane angle study.

Acknowledgments

The authors would like to thank the personnel of the Duits-Nederlandse Wind Tunnel for superb support at every level. Sincere appreciation is extended to all our colleagues at DFVLR Braunschweig Research Center, NASA Langley Research Center, and the Army Aerostructures Directorate as well.

References

[1]Charles, B. D., "Acoustic Effects of Rotor-Wake Interaction During Low Power Descent," *Proceedings of National Symposium on Helicopter Aerodynamic Efficiency*, American Helicopter Society, Alexandria, VA, 1975, pp. 7.1–7.8.

[2]Shockey, G. A., Williams, J. W., and Cox, C. R., "Helicopter Aerodynamics and Structural Loads Survey," *Proceedings of 32nd Annual National V/STOL Forum*, American Helicopter Society, Alexandria, VA, May 1976, Preprint 1060.

[3]Boxwell, D. A. and Schmitz, F. H., "Full Scale Measurements of Blade-Vortex Interaction Noise," *Proceedings of the 36th Annual Forum*, American Helicopter Society, Alexandria, VA, May 1980, Preprint 80–61.

[4]Splettstoesser, W. R., Schultz, K. -J., Boxwell, D. A., and Schmitz, F. H., "Helicopter Model Rotor-Blade-Vortex Interaction Impulsive Noise: Scalability and Parametric Variations," NASA TM 86007, Dec. 1984.

[5]Schlinker, R. H. and Amiet, R. K., "Rotor-Vortex Interaction Noise," NASA CR 3744, Oct. 1983.

[6]Leighton, K. P. and Harris, W. L., "On Mach Number Scaling of Blade-Vortex Noise Produced by Model Helicopter Rotors at Moderate Tip Speeds," Dept. of Aeronautics and Astronautics, M.I.T., Cambridge, MA, Rept. 84–3, Oct. 1984.

[7]Martin, R. M., Elliott, J. W., and Hoad, D. R., "Comparison of Experimental and Analytical Predictions of Rotor Blade-Vortex Interactions Using Model Scale Acoustic Data," AIAA Paper 84–2269, Oct. 1984.

[8]Hoad, D. R., "Helicopter Blade-Vortex Interaction Locations—Scale-Model Acoustics and Free-Wake Analysis Results," NASA TP 2658, 1987.

[9]Martin, R. M. and Splettstoesser, W. R., "Acoustic Results of the Blade-Vortex Interaction Test of a 40 Percent Model Rotor in the DNW," *Proceedings of National Specialist's Meeting on Aerodynamics and Aeroacoustics*, American Helicopter Society, Alexandria, VA, Feb., 1987.

[10]Martin, R. M., Splettstoesser, W. R., Elliott, J. W., and Schultz, K.-J., "Acoustic Measurements from a Model Rotor Blade-Vortex Interaction Noise Experiment in the German-Dutch Wind Tunnel (DNW)," NASA TM 4027, U.S. Army Aviation Systems Command, Hampton, VA, AVSCOM TR 87-B-4, 1988.

[11]Egolf, T. A. and Landgrebe, A. J., "Helicopter Rotor Wake Geometry and Its Influence in Forward Flight, Volume I—Generalized Wake Geometry and Wake Effects on Rotor Airloads and Performance," NASA CR 3726, 1983.

[12]Egolf, T. A. and Edwards, D., "Users Manual for a Stand-Alone Version of the UTRC Generalized Wake Module," United Technologies Research Center, East Hartford, CT, UTRC Rept. R83–912666–57, 1983.

[13]Langer, H. J., "DFVLR Rotorcraft-Construction and Engineering," NASA TM 77740, Aug. 1984.

[14]Langer, H. J., "Data Input, Processing and Presentation," NASA TM 77739, July 1984.

[15]Breustedt W., "Data Analysis at a Rotor Test Stand Program for Interactive Analysis," NASA TM 77948, Nov. 1985.

[16]Heyson, H. H., "Use of Superposition in Digital Computers to Obtain Wind Tunnel Interference Factors for Arbitrary Configurations, with Particular Emphasis to V/STOL Model," NASA TR R–302, Feb. 1969.

[17]Boxwell, D. A., Schmitz, F. H., Splettstoesser, W. R., and Schultz, K.-J., "Model Helicopter Rotor High Speed Impulsive Noise: Measured Acoustics and Blade Pressures," NASA TM 85850, Sept. 1983.

[18]Splettstoesser, W. R., Schultz, K.-J., and Martin, R. M., "Rotor Blade-Vortex Interaction Impulsive Noise Source Identification and Correlation with Rotor Wake Predictions," AIAA Paper 87–2744, Oct. 1987.

[19]Bliss, D. B., Dadone, L., and Wachpress, D. A., "Rotor Wake Modeling for High Speed Applications," *Proceedings of 43rd Annual Forum*, American Helicopter Society, Alexandria, VA, Vol. 1, May 1987, pp. 17–33.